Title: DEPOSITION OF HYDROXYAPATITE AND TRICALCIUM PHOSPHATE COATINGS BY SUSPENSION PLASMA SPRAYING: EFFECTS OF TORCH SPEED

Authors: I. Ročňáková, K. Slámečka, E.B. Montufar, M. Remešová, L. Dyčková, A. Břínek, D. Jech, K Dvořák, L. Čelko, J. Kaiser

PII: S0955-2219(18)30493-X
DOI: https://doi.org/10.1016/j.jeurceramsoc.2018.08.007
Reference: JECS 12032

To appear in: *Journal of the European Ceramic Society*

Received date: 13-4-2018
Revised date: 20-7-2018
Accepted date: 4-8-2018

Please cite this article as: Ročňáková I, Slámečka K, Montufar EB, Remešová M, Dyčková L, Břínek A, Jech D, Dvořák K, Čelko L, Kaiser J, DEPOSITION OF HYDROXYAPATITE AND TRICALCIUM PHOSPHATE COATINGS BY SUSPENSION PLASMA SPRAYING: EFFECTS OF TORCH SPEED, *Journal of the European Ceramic Society* (2018), https://doi.org/10.1016/j.jeurceramsoc.2018.08.007

DEPOSITION OF HYDROXYAPATITE AND TRICALCIUM PHOSPHATE COATINGS BY SUSPENSION PLASMA SPRAYING: EFFECTS OF TORCH SPEED

I. Ročňáková[1*], K. Slámečka[1], E.B. Montufar[1], M. Remešová[1], L. Dyčková[1], A. Břínek[1], D. Jech[1,], K Dvořák[2], L. Čelko[1], J. Kaiser[1]

[1]CEITEC – Central European Institute of Technology, Brno University of Technology, Brno, Czech Republic.

[2]Faculty of Civil Engineering, Brno University of Technology, Brno, Czech Republic.

*Corresponding author

Address: CEITEC – BUT, Purkyňova 656/123, Brno 612 00, Czech Republic

E-mail address: ivana.rocnakova@ceitec.vutbr.cz

Tel.: (+420) 54114 9877, (+420) 721 016 644

Abstract

This research focuses on the deposition of hydroxyapatite (HA) and tricalcium phosphate (TCP) coatings produced by suspension plasma spraying (SPS) using in-house liquid feedstock suspensions. The work studied the effects of torch speed on the thickness, microstructure, and crystalline composition of the coatings. SPS allowed the deposition of HA and TCP coatings with thickness between 28 and 90 μm. The coatings presented lamellar microstructure with complex porosity between the splats. Micropores ranging from 0.2 to 6 μm and close mesopores, from 8 to 45 μm, had a spherical morphology and were homogenously distributed within the coatings. Water evaporation during SPS allowed the

retention of pure and crystalline HA coatings. In contrast, the presence of water molecules led to the formation of HA as a secondary phase in the TCP coatings, which formed α-TCP as the major component due to the high temperature reached by the powder during deposition.

Keywords: suspension plasma spraying; hydroxyapatite; tricalcium phosphate; porosity; x-ray computed micro-tomography

1. Introduction

Deposition of bioactive coatings on metallic prosthesis is one of the most successful approaches to improve osseointegration of orthopaedic implants [1]. The bioactive coatings prevent the formation of fibrous layer at the implant-bone interface, suppressing micromovements which can lead to the failure of the implant. The most common material deposited is hydroxyapatite (HA, $Ca_{10}(PO_4)_6(OH)_2$). Several techniques can be used to produce HA coatings, including electrochemical deposition [2], sol-gel method [3], precipitation in simulated body fluid [4], and atmospheric plasma spraying (APS), among others. APS is the most commercially accepted technique for the deposition because of its high productivity, relatively low costs and moderate heat transferr to the substrate [5]. In the conventional APS process, the powder is injected by gas into the plasma flame and the particles are melted, while being projected at high speeds towards the surface of the substrate [6]. Nonetheless, APS has the drawback that it commonly causes the chemical decomposition of HA due to the high temperature of the process, leading to secondary phases detrimental to the mechanical and biological performance of the coating. In particular, the formation of CaO, which reacts with water molecules to produce $Ca(OH)_2$ connected with considerable increase of volume, is one of the most problematic issues because it causes cracking and delamination of the coating [7-8]. Recently, a modification of APS was introduced known as suspension plasma spraying (SPS) that allows the injection of submicrometer sized powder particles and the preparation of new and unique types of structures [9]. In this method, the powder is injected into the plasma as a suspension, thus avoiding problems associated with powder flowability. The SPS process involves many variables, including suspension concentration, injection conditions, and plasma enthalpy and its flow rate, which affects suspension break-up and movement, enabling a variety of microstructures ranging from feathery to dense lamellar coatings similar to those produced by APS [10, 11]. More importantly, the use of water-base

suspensions prevents the dehydration of HA during deposition and allow the formation of pure HA coatings with no secondary phases [12].

Other calcium phosphate that can be used as a bioactive coating is tricalcium phosphate (TCP). In fact, TCP is one of the phases produced by the decomposition of HA during coating deposition by APS [13]. TCP coatings are narrowly studied because of their higher solubility with respect to HA, a property that may cause failure of the implant at the coating-substrate interface but at the same time is advantageous for instance in temporal protection of biodegradable magnesium orthopaedic implants against early corrosion and their timed degradation once the bone is healed.

Only few works have explored the deposition of HA and TCP coatings by the conventional APS process with the aim to study the dissolution behaviour [14]. To the best of our knowledge, the deposition of pure TCP coatings by SPS has not been studied yet. TCP has three polymorphs; (i) the β-TCP phase stable at room temperature, (ii) the α-TCP phase stable above 1180 °C and (iii) the α´-TCP phase stable above 1430 °C [15]. The α-TCP is slightly more soluble than β-TCP and the preservation of this phase can lead to coatings that degrade in a shorter time. In addition to the chemical composition of the coating, another parameter used to control the degradation rate is the thickness of the coating. In the case of the SPS method, the thickness mainly depends on the powder content in the suspension, suspension feeding rate and the torch speed. In particular, the last parameter is quite relevant because it also remarkably affects the heat transfer to the substrate, the cooling rate and, therefore, the phases produced in the coating and the substrate. This paper specifically investigates the effects of torch speed on the microstructure, composition and thickness of HA and TCP coatings deposited by SPS. Furthermore, the possibility of controlling the porosity and

thickness of coatings by using different torch speed was addressed. To this end, all processing parameters were fixed and the torch speed was varied between 50 and 500 mm/s.

2. Materials and methods

2.1 Calcium phosphate powders and suspension preparation

HA was synthetized by a well-established wet precipitation method [16]. The orthophosphoric acid (85 %, analytic grade, Lach-ner s.r.o.) solution was added drop by drop into calcium hydroxide (analytic grade, Lach-ner s.r.o.) solution under constant agitation at room temperature. The addition of orthophosphoric acid was stopped when the solution attained a pH of 9.0 and was followed by maturation under agitation for 12 h. The product was then filtered and dried at 100 °C, after which the produced HA block was manually grinded in a mortar and milled for 10 min using a high energy ball mill (Simoloyer CM01, ZoZ). In contrast, the β-TCP suspension used in this work was prepared using a commercially available powder (VWR Chemicals). Powder aggregates were reduced by milling for 10 min. The particle size distribution of both powders was measured before and after milling by laser diffraction (Mastersizer 2000, Malvern).

The morphology of powders was characterized by scanning electron microscope (SEM; Lyra3, Tescan). The crystalline composition was determined by X-ray diffraction (XRD) analysis (Panalytical Empyrean) using Cu K-α radiation (45 mA and 40 kV) and the measurement step of 0.013° in 2θ with the scan rate of 150 s per step. Phase analysis was performed using High Score+ software based on the Inorganic Crystal Structure Database (ICSD).

The liquid suspension feedstocks were produced by adding 100 g of either HA or β-TCP milled powders into 1 L of a 1:1 mixture of distilled water and isopropanol (1:1). Powders

were homogenously dispersed in the liquid by probe sonication (Sonopuls UW 3400, Bandelin) for 5 min followed by mechanical stirring for 10 min.

2.2 Deposition of the coatings by suspension plasma spraying

The coatings were deposited on steel (ISO 683-1-87) disc with diameter of 20 mm and thickness of 10 mm. Prior to the deposition, the discs were mechanically polished, ultrasonically cleaned in ethanol, dried in hot air, blasted (OTECO cabin) with acicular Al_2O_3 particles of grain size F 14, cleaned and then dried again. The coatings were deposited by atmospheric SPS process using the F4 MB-XL plasma spray torch (Sulzer Metco) mounted on an automatic robot (IRB 2600, ABB). The spraying parameters were selected with respect to the deposition efficiency and are listed in Table 1. In this study, the attention was focused on the torch speed which was varied (50, 200, and 500 mm/s) and all other parameters were kept constant. In-flight behavior of particles was studied using AccuraSpray G3C ensemble sensor (Tecnar Automation, Canada) designed for online monitoring and controlling of thermal spray processes. The sensor provides average values of velocity and temperature of particles from 3.2 mm diameter × 25 mm depth of field (perpendicular to the particle stream) volume. The data were collected using 15 s monitoring runs.

Table 1 SPS parameters.

Torch speed	50, 200, and 500 mm/s
Primary plasma gas (Ar) flow rate	45 slpm*
Secondary plasma gas (H) flow rate	5 slpm*
Arc current	530 A

Standoff distance	85 mm
Suspension pressure	1 bar
Suspension feed rate	25 g/min

*slpm: standard litres per minute

2.3 Coatings characterization

The crystalline phase composition of the coatings was determined by XRD analysis as described above. Metallographic samples for microstructural analysis were prepared by low-speed cutting, grinding by increasingly finer sandpaper (up to #2000), mechanical polishing by 3 and 1 µm diamond paste, and chemical polishing using OP-S silica solution. The mounting pressure as well as the polishing pressure were reduced to avoid cracking at weak regions in the coating. Samples were examined with SEM; prior to observation, the samples were coated with a fine carbon layer to prevent charging during the images recording.

2.4 Analysis of thickness and porosity

Thickness of the coatings was determined from three-dimensional (3D) virtual reconstruction of X-ray computed micro-tomography (µCT) images. Two ranges of pore size were defined for the analysis of porosity and pore size distribution. Mesopores were defined as pores of size above 8 µm (quadruple of the µCT voxel resolution of 2 µm), while micropores not observable by µCT were defined as pores of size below 8 µm. Micropores were studied *via* SEM image analysis (SEM-IA) using the OLYMPUS Stream software and backscattered electron (BSE) images to increase the contrast between pores and material. The microporosity (the ratio of the total area of pores to the total area of the region of interest) was determined based on at least 10 images per each sample.

Mesopores were studied *via* µCT. X-ray computed micro-tomography was performed using the system GE phoenix v|tome|x L 240 (GE Sensing & Inspection Technologies GmbH, Germany) equipped with 180 kV/15 W nanofocus X-ray tube and flat panel detector DXR 250. The X-ray tube was set at accelerating voltage of 120 kV and current of 70 µA, and used at focus mode 1, keeping the source spot size at 2 µm. The X-ray spectrum was filtered by 0.2 mm thick copper filter. The detector exposure time was 500 ms in every of 2200 positions. The voxel resolution of the obtained µCT data was 2 µm. The measurement was performed at the constant temperature of 21 °C.

The tomographic reconstruction was performed using GE phoenix datos|x 2.0 software with the sample drift and beam hardening corrections. The µCT data analysis and visualisation was performed by VG Studio MAX 3.0 (Volume Graphics GmbH, Germany). The contrast between the coating layer and the steel substrate was sufficient to segment the layer using the automatic thresholding. Conversely, the interface between the coating and metallographic resin has a low contrast and the manual thresholding method was implemented. The defect determination and wall thickness determination modules within VG Studio were subsequently applied on the segmented coating layer to calculate the mesoporosity (the ratio of the total volume of pores to the total volume of the coating), pore size distribution, the sphericity of the pores (the ratio of the surface of a sphere of the same volume as the pore to the surface of the pore), and the thickness of the coatings. The modules were set for *only threshold algorithm*, filtering out objects smaller than 16 voxels cluster. The threshold value was chosen manually by the operator based on visual evaluation of representative cross-sections.

3. Results

3.1 Powders characterization

Figure 1 shows the particle size distributions for both HA and β-TCP powders. The size distribution of hand-grinded (initial) HA was broad. The milling did not reduce the powder size (average around 20 μm), but narrowed the distribution by mainly decreasing the size of the bigger particles. The initial particle size distribution of the commercial β-TCP powder presented a bimodal distribution with a distinct peak around 1 mm, probably due to powder aggregation. After milling, this peak disappeared and the particle size distribution became narrower with particles between 0.5 and 50 μm. Powders after milling were selected for SPS because the narrow particle size distribution with smaller particles is preferred in order to improve the flowability of the suspension.

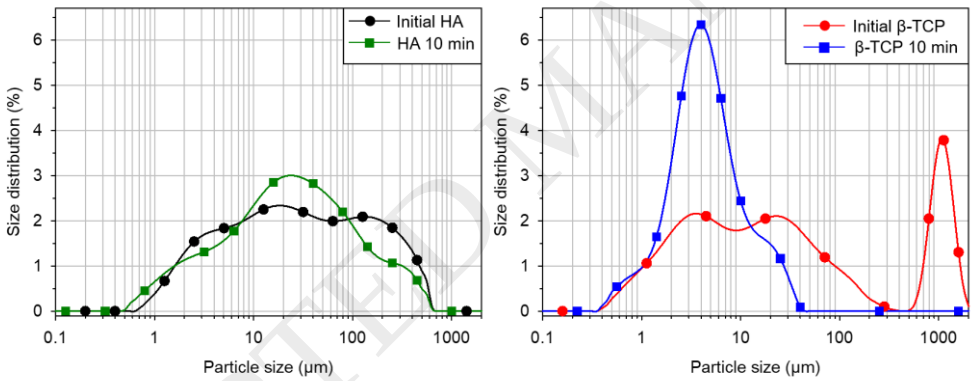

Figure 1. Particle size distribution of the initial HA and β-TCP powders and those after milling for 10 min.

The surface morphology of the powder particles after milling is shown in Figure 2. The HA powder particles were aggregates of tinny nanocrystals, around 100 nm in size. Similar morphology was observed for β-TCP particles. The crystalline composition of the powders is revealed in Figure 3, together with the crystalline composition of deposited coatings. The XRD pattern of the HA powder fitted with the reference pattern of HA. Nonetheless, wide

diffraction peaks suggest the small size of crystalline domains in the HA powder particles, corresponding well with SEM observations. The initial composition of the commercial β-TCP powder did not correspond entirely with β-TCP crystalline phase and the experimental XRD pattern of this powder was indexed as calcium hydrogen phosphate anhydrides ($CaHPO_4$) with HA and β-TCP.

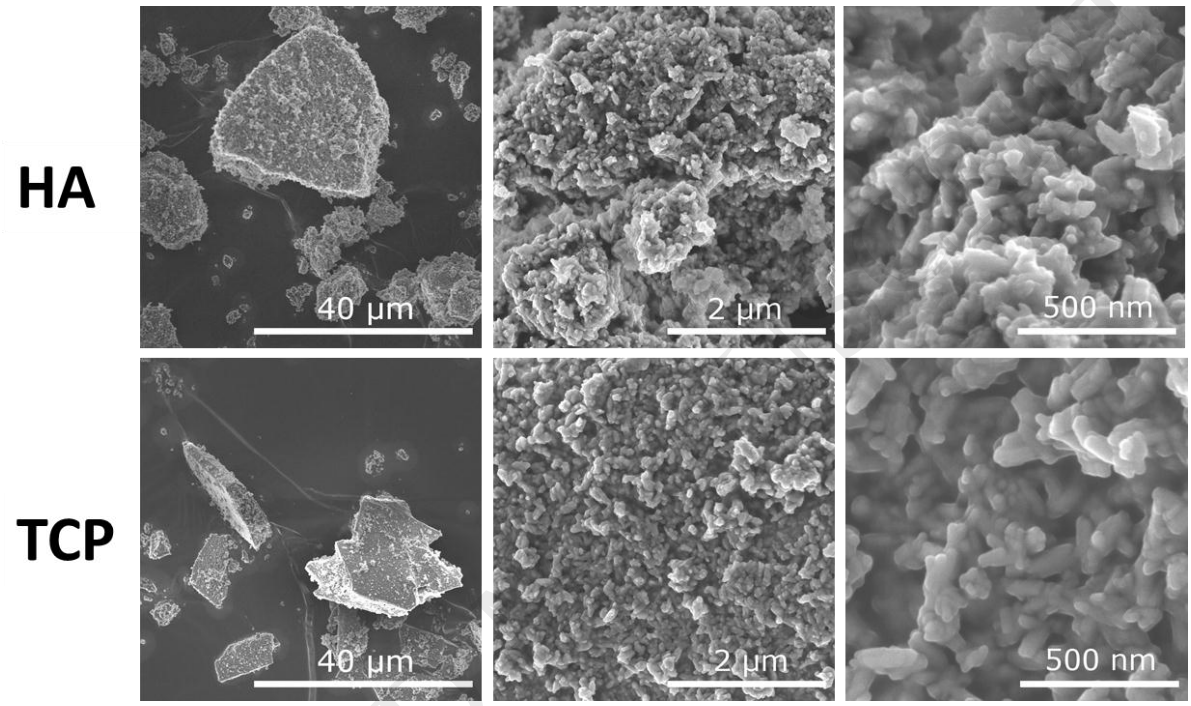

Figure 2. Representative secondary electron SEM images of the milled HA and β-TCP powders.

3.2 Crystalline composition of the coatings

The average temperature and velocity of particles impacting the substrate was, respectively, 1851 ± 14 °C and 288 ± 5 m/s, independent of the feedstock material. The crystalline composition of produced HA coatings corresponded to pure HA withno secondary phases (Figure 3). In comparison with the initial milled HA powder, the HA coatings presented more discernible peaks, indicating increased size of crystalline HA domains. The intensity of the diffraction peaks was related to the torch speed, the lower torch speed resulting in higher

intensity of the peaks. This effect was more significant between the torch speed of 50 and 200 mm/s than between 200 and 500 mm/s.

The TCP coatings presented important differences in crystalline composition with respect to the milled powder used for their deposition. The coatings were composed mainly of α-TCP with HA and β-TCP as secondary phases. No other phases, such as CaO, were detected in neither the HA nor the TCP coatings. Similarly to HA coatings, the intensity of the diffraction peaks of the TCP coatings was higher for lower torch speeds. Furthermore, the XRD patterns of both HA and TCP coatings deposited at the highest studied torch speed (500 mm/s) presented the characteristic peaks of iron, which is related to the low thickness of coatings and represents the underlying steel substrate.

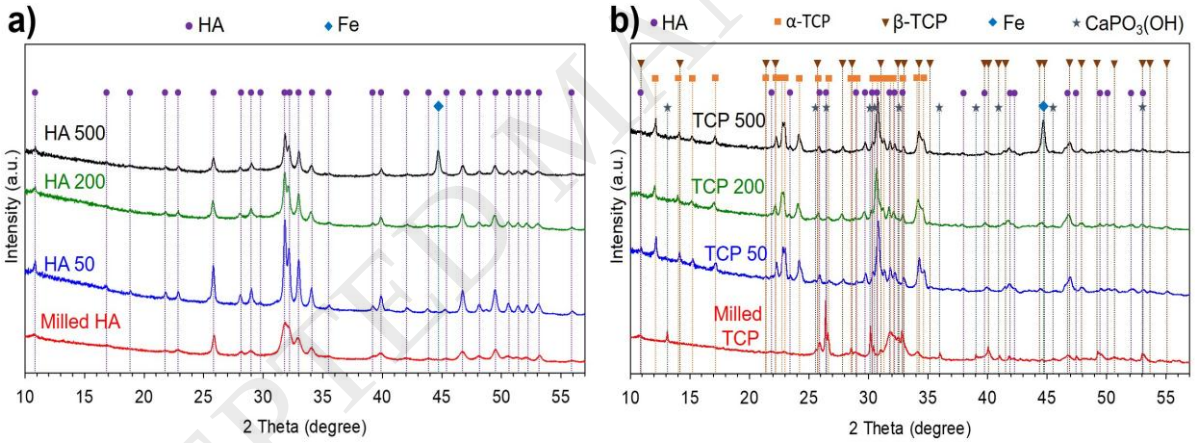

Figure 3. XRD paterns of a) HA and b) TCP milled powders and coatings deposited at different torch speeds.

3.3 Microstructure and thickness of the coatings

Figure 4 shows representative images of coatings deposited at different torch speeds. The coatings were highly porous and had the lamellar microstructure formed by flat splats suggesting complete melting of both HA and TCP particles during the SPS process.

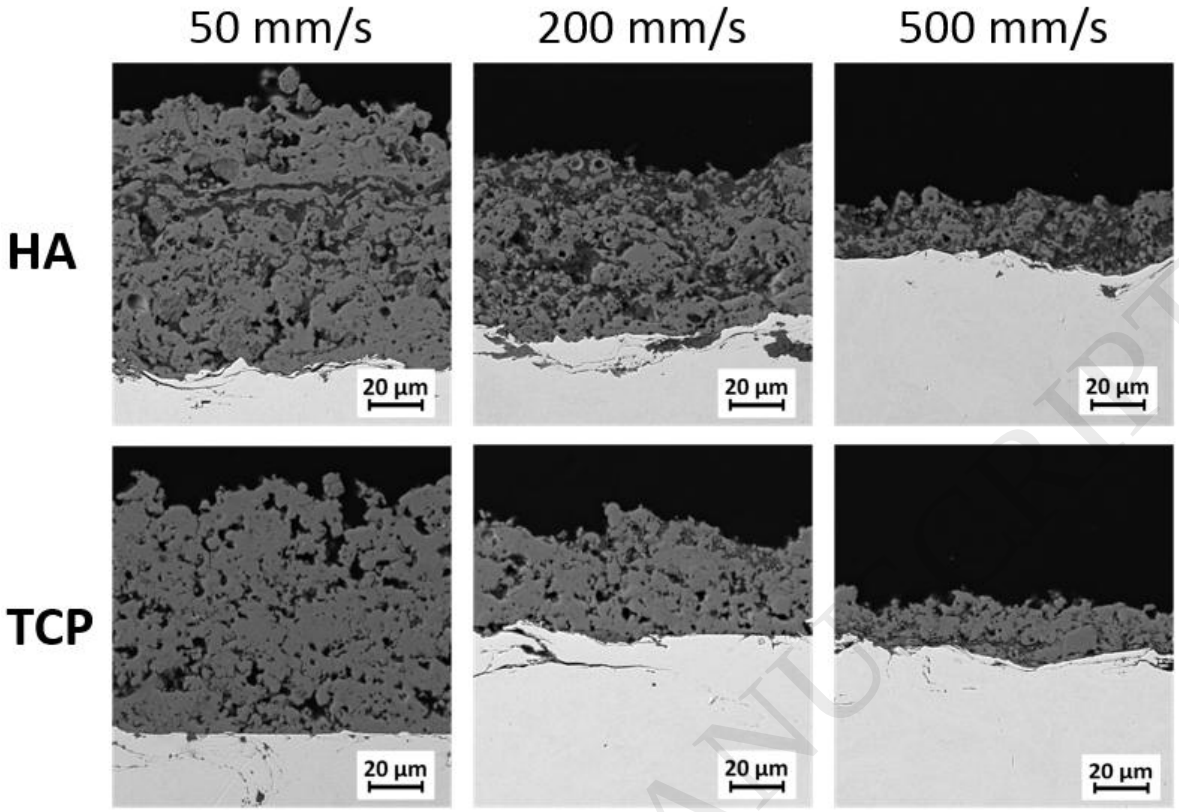

Figure 4. Representative backscattered electrons SEM images of HA and β-TCP coatings deposited at different torch speeds.

Coatings with average thickness between 28 and 90 µm were obtained following the processing parameters used in this work, Figure 5. The thickness of the coatings decreased significantly with increasing torch speed. Similarly, the variation of thickness decreased with increasing torch speed. Thickness of HA and TCP coatings deposited at 500 mm/s was not statistically significantly different, unlike at lower torch speeds.

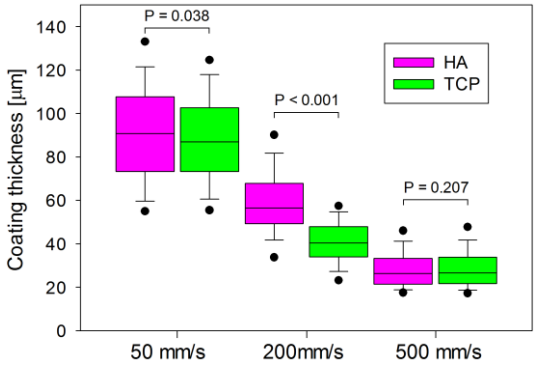

Figure 5. Thickness of the HA and β-TCP coatings deposited at different torch speeds.

3.4 Porosity of the coatings

Figure 6 and 7 show virtual 3D reconstruction of μCT data; the bottom and middle images are, respectively, the substrate and the coating with mesopores shown in gold colour, which are also presented separately in the top images. The mesopores were closed (not interconnected), homogeneously distributed within the coating and have the average sphericity of 0.44 ± 0.07. More detailed observation of samples with coatings deposited at the highest torch speed (500 mm/s) revealed some uncoated areas, especially in the case of TCP coatings. This is in agreement with the results of XRD that revealed the characteristic peaks for iron in these thin coatings.

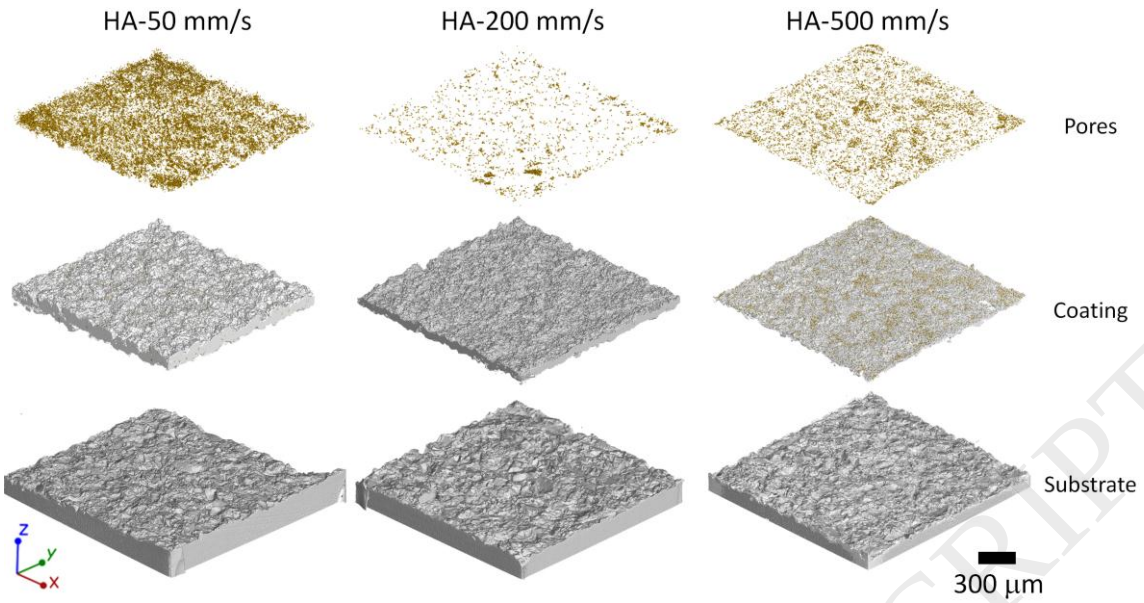

Figure 6. Representative 3D reconstructions of µCT data obtained from samples coated with HA at different torch speeds. The images in the top row show the mesopores within the coating layer.

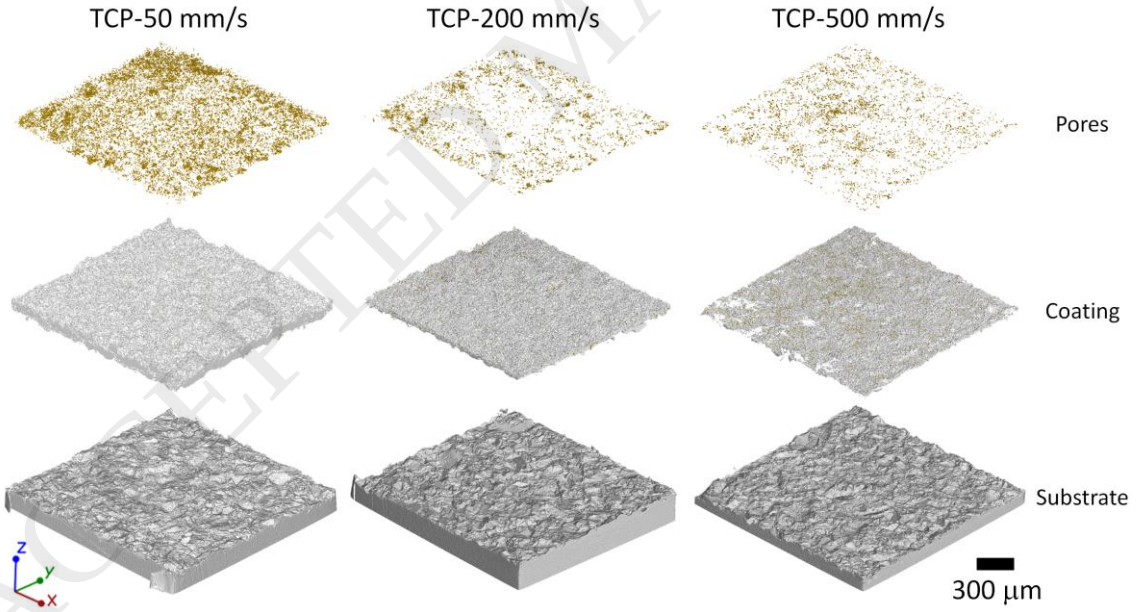

Figure 7. Representative 3D reconstructions of µCT data obtained from samples coated with TCP at different torch speeds. The images in the top row show the mesopores within the coating layer.

The percentage of porosity determined by SEM-IA and μCT is presented in Figure 8. The microporosity determined by SEM-IA was significantly higher than mesoporosity determined by μCT. This indicates that most of the pores had sizes below 8 μm. The microporosity was distinctly lower for the TCP coatings than for the HA coatings and generally decreased with increasing torch speed. The mesoporosity was similar for HA and TCP coatings deposited at the torch speeds of 50 and 200 mm/s and it was somewhat higher for the HA coatings than the TCP coatings deposited at the highest torch speed of 500 mm/s. For both coatings, the mesoporosity presented a minimum at the torch speed of 200 mm/s.

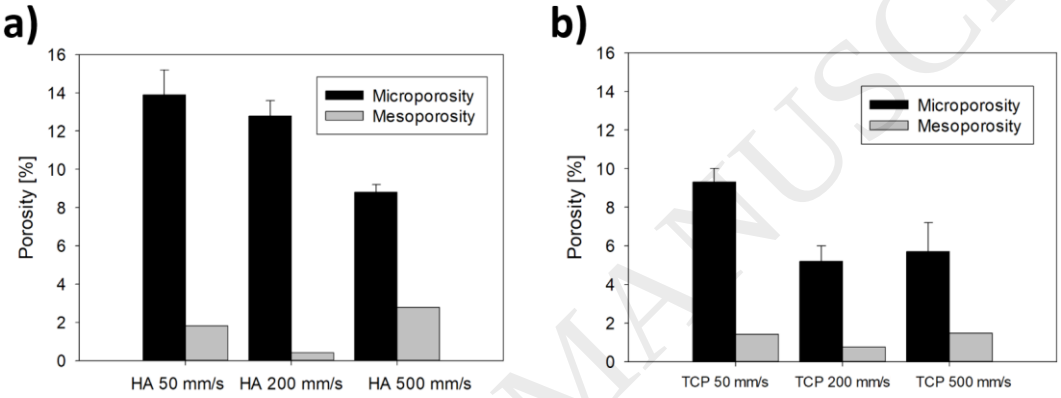

Figure 8. Porosity determined by SEM-IA (micropores) and μCT (mesopores) for a) HA and b) TCP coatings deposited at different torch speeds.

The pore size distributions are presented in Figure 9. Both methods (SEM-IA and μCT) provided complementary information about the pores. For the torch speed of 50 mm/s, the size of the micropores ranges from 0.8 to ~6 μm and that of the mesopores ranges from 8 to ~45 μm. The pores are generally somewhat smaller for higher torch speeds (200 and 500 mm/s). The size distribution of micropores in the HA coatings was centred on ~1.5 μm and that of mesopores was centred on ~13 μm. Similarly, the size of the mesopores in the TCP coatings was centred on 13 μm. Nonetheless, the size distribution of micropores in the TCP

coatings was considerable shifted to smaller size (below 1 μm) for higher torch speeds (200 and 500 mm/s).

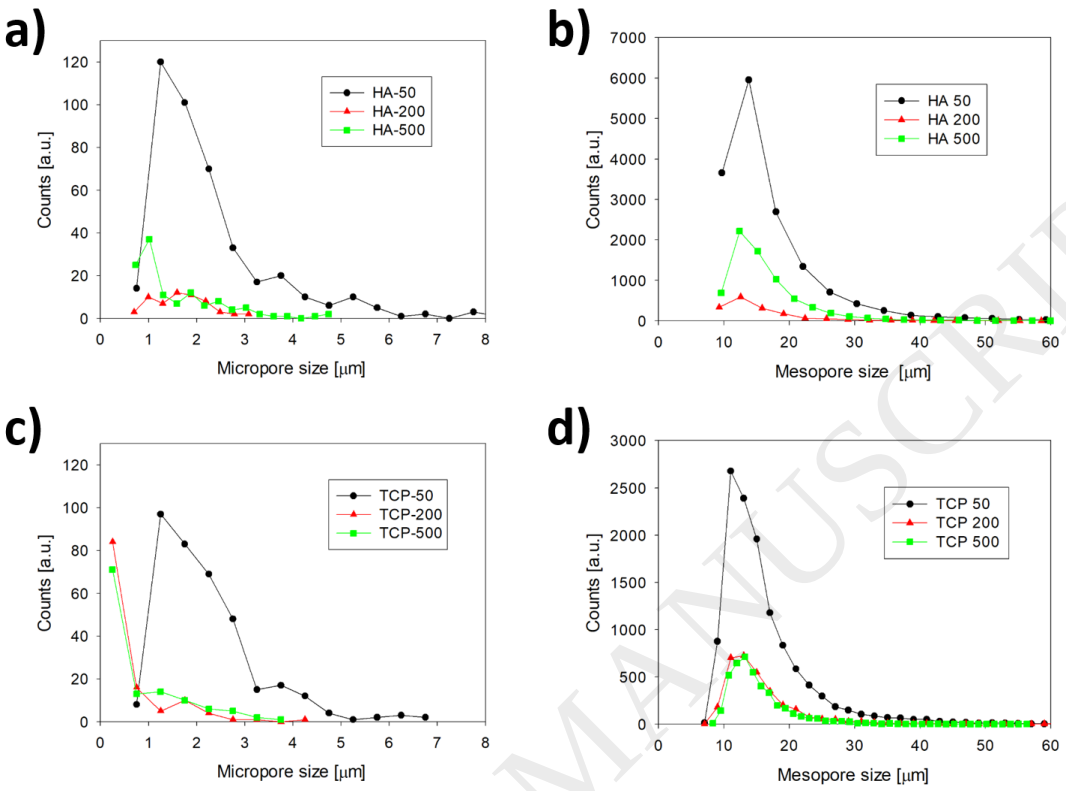

Figure 9. The influence of the torch speed on the pore size distribution for a-b) HA coatings and c-d) TCP coatings. Graphs a), c) show the micropore size distribution determined by SEM-IA and graphs b), d) show the mesopore size distribution determined by μCT analysis.

4. Discussion

HA and TCP coatings were successfully deposited by the SPS method. HA retained its composition after deposition. This was due to the evaporation of water that provides a moisture environment which prevents the decomposition of HA into non-hydrated phases, such as TCP and tetracalcium phosphate [17]. The SPS of TCP is much more complex than for HA. The initial $CaHPO_4$ and HA mixture reacted during coating deposition to produce α-

TCP coatings containing β-TCP and HA as the secondary phases. The chemical reaction involved in the synthesis of TCP during SPS can be written as follows:

Synthesis:

$2CaHPO_4 + Ca_{10}(PO_4)_6(OH)_2 \rightarrow 4Ca_3(PO_4)_2 + 2H_2O$

The synthesis reaction of TCP is instantaneous at temperature above 900 °C [18]. The specific TCP polymorph formed depends on the temperature of the reaction. Since in the present study the particles reached the temperature of 1850 °C, the α´-TCP phase should be formed. However, during cooling and below 1430 °C, the α´ phase immediately transforms to the α phase. In contrast, the α-TCP to β-TCP phase transformation is reconstructive [19, 20], which means that the transformation involves major reorganization of the crystalline structure with the breaking and formation of several chemical bonds [21]. Therefore, the reversion from α-TCP to β-TCP phase requires large dwell time at temperatures slightly below 1180 °C. In fact, it has been shown that pure α-TCP can be retained at cooling rates as low as 10 °C/min [18, 19, 22]. It is difficult to determine the exact cooling rate during deposition of coatings studied in this work, but it is considered to be in the range of several degrees Celsius per second [23, 24]. Accordingly, the main crystalline phase in the TCP coating correspond to the α-TCP polymorph.

The presence of β-TCP in these coatings is due to the presence of this crystalline phase in the powder feedstock. Despite the temperature of the process, the high energy required for the β-TCP to α-TCP transformation, together with short processing time, does not allow the equilibrium and the content of β-TCP was thus almost invariant in all the samples (around 10 %).Similarly to HA, the evaporation of water from the liquid suspension caused the hydration

of TCP leading to the formation of HA third phase. The chemical reaction associated with the hydrolysis of TCP into HA is the following:

Hydrolysis:

$3Ca_3(PO_4)_2 + H_2O \rightarrow Ca_9(HPO_4)(PO_4)_5(OH)$

The torch speed had an important effect on the crystallinity of the deposited HA and TCP coatings as evidenced by higher intensity of diffraction peaks at lower torch speeds. This is because the lower speed increases the exposure time of the deposited coating to the hot plasma, thus promoting the heat transfer, and therefore, providing more energy for recrystallization and grain growth. Despite that the intensity of the diffraction peaks of coatings deposited at higher speeds is somewhat lower, the XRD results still revealed the crystalline nature of the coatings. The effects on the coating crystallinity are relevant since it is well accepted that the crystallinity of the calcium phosphates has a paramount effect on their solubility [25-26]. Therefore, the torch speed should be considered in the development of coatings with well-controlled dissolution rates.

In general, the thickness of the TCP coatings was slightly lower than the thickness of the HA coatings deposited at the same torch speed. Since the powder content of the suspensions used in this work was the same, the difference can be attributed to better densification of the TCP particles during the splat formation. In fact, the TCP coatings contained fewer micropores and mesopores than the HA coatings. The current trend in research and industrial practice is to manufacture thin coatings, which have homogeneous structure without significant defects [27]. The thinner coatings usually contain lower residual stresses, decreasing the risks of cracking, delamination, and spalling [28]. Following the processing

conditions used in this work, coatings with a minimum mean thickness of 28 µm can be obtained by SPS. Such low thicknesses are difficult to achieve by the conventional APS method and the possibility of depositing thin coatings represents one of the advantages of SPS. Nonetheless, the thinnest coatings studied in this work presented some areas where the metallic substrate was partially exposed. This is the drawback in particular if the coating should protect the implant from corrosion. Possible solutions are increasing the powder content of the suspension or depositing coatings at slightly lower torch speed. It is worth to mention that the thickness of the coating decreases with increasing torch speed and, therefore, the torch speed somewhat lower than 500 mm/s should be studied in order to retain thin coatings but with no discontinuities.

With respect to the porosity, the coatings deposited by the SPS method are complex materials, containing pores at different scales. Because of this, the porosity was quantified in this work using two complementary methods, i.e. SEM-IA and µCT. We proven that higher torch speeds (200 and 500 mm/s) produced somewhat smaller pores at both micro- and meso-scales than the torch speed of 50 mm/s. X-ray computed micro-tomography tomography allows a more comprehensive characterization of the porosity than SEM-IA. Nonetheless, most of the porosity was below the detection limit of µCT and it was not possible to study the micropores within the coatings using this method. Mesopores were found to be homogenously distributed within the coatings and had a quasi-spherical morphology. They were closed, which means that there is no connection between the surface of the coating and the substrate-coating interface. This is relevant in order to prevent localized corrosion of the substrate by infiltration of water molecules. Nonetheless, the study of the corrosion protective effects of the coatings was not the objective of this work. Unpublished work is ongoing in this direction in our laboratories, with the aim to temporally protect magnesium and magnesium alloys

against corrosion. In addition, the mesoporosity in the coatings can improve the osseointegration of the coated substrate [29-30]. This is an important effect in order to provide mechanical stability to the bone during the time required for healing. The total porosity of the HA coatings was higher than the porosity of commercially available ceramic coatings, which is usually less than 10 % [31-32]. In contrast, the total porosity of the TCP coatings was within this reference value.

5. Conclusions

The torch speed demonstrated important effects on the thickness, porosity and crystallinity of the HA and TCP coatings deposited by the SPS method, but did not affect significantly the pore size distribution or the morphology of the mesopores. The thickness of the coatings can be controlled between 28 and 90 μm, following the processing parameters used in this work. The microporosity generally decreased with the torch speed while the mesoporosity presented a minimum at torch speed of 200 mm/s. The TCP coatings were less porous than the HA coatings. HA did not decompose during coating deposition, leading to coatings with no secondary phases. The mixture of $CaHPO_4$ and HA reacted during SPS to form α-TCP. Nonetheless, the moisture atmosphere created by the evaporation of water from the suspension hydrolized TCP to form HA as a secondary phase in the TCP coatings. The initial content of β-TCP in the powder feedstock was maintained constant in the deposited coatings. Finally, the intensity of the diffraction peaks of the coatings was higher for coatings deposited at lower torch speed.

6. Acknowledgements

This project has received funding from the European Union's Horizon 2020 research and innovation programme under the Marie Skłodowska-Curie and it is co-financed by the South Moravian Region under grant agreement no. 665860. Authors also acknowledge the project CEITEC 2020 (LQ1601) with financial support from the Ministry of Education, Youth and Sports of the Czech Republic under the National Sustainability Program II. Acknowledgements also to the project CEITEC Nano Research Infrastructure (ID LM2015041, MEYS CR, 2016–2019) for providing use with access to its devices used for this research.

References

[1] DURDU, S., USTA, M., BERKEM, Al.S. Bioactive coatings on Ti6Al4V alloy formed by plasma electrolytic oxidation. *Surface and Coatings Technology*. 2016, 301, 85-93.

[2] NARAYANAN, R., SESHADRI, S.K., KWON, T.Y., KIM, K.H. Electrochemical nano-grained calcium phosphate coatings on Ti–6Al–4V for biomaterial applications. *Scripta Materialia*. 2007, 56, 229-232.

[3] BEN-NISSAN, B., A. MILEV, R., VAGO, R. Morphology of sol–gel derived nano-coated coralline hydroxyapatite. *Biomaterials*. 2004, 25, 4971-4975.

[4] BIGI, A., BOANINI, E., BRACCI, B., FACCHINI, A., PANZAVOLTA, S., SEGATTI, F., STURBA, L. Nanocrystalline hydroxyapatite coatings on titanium: a new fast biomimetic method. *Biomaterials*. 2005, 26, 4085-4089.

[5] SURMENEV, R. A review of plasma-assisted methods for calcium phosphate-based coatings fabrication. *Surface and Coatings Technology*. 2012, 206, 2035-2056.

[6] LEI, S., YAN-FENG, X., LU, G., YAO, W., FANG, W., ZHONG-WEI, G. The effect of antibacterial ingredients and coating microstructure on the antibacterial properties of plasma sprayed hydroxyapatite coatings. *Surface and Coatings Technology*. 2012, 206, 2986-2990.

[7] HABERKO, K., BUĆKO, M.M., BRZEZIŃSKA-MIECZNIK, J., HABERKO, M., MOZGAWA, W., PANZ, T., PYDA, A., ZARĘBSKI, J. Natural hydroxyapatite—its behaviour during heat treatment. *Journal of the European Ceramic Society*. 2006, 26, 537-542.

[8] OTSUKA, Y., KOJIMA, D., MUTOH, Y. Prediction of cyclic delamination lives of plasma-sprayed hydroxyapatite coating on Ti–6Al–4V substrates with considering wear and dissolutions. *Journal of the Mechanical Behavior of Biomedical Materials*. 2016, 64, 113-124.

[9] CARNICER, V., ALCAZAR, C., SÁNCHEZ, E., MORENO, R. Aqueous suspension processing of multicomponent submicronic Y-TZP/Al2O3/SiC particles for suspension plasma spraying. *Journal of the European Ceramic Society*. 2018, 38, 2430-2439,

[10] SESHADRI, R.CH., DWIVEDI, G., VISWANATHAN, V., SAMPATH, S. Characterizing Suspension Plasma Spray Coating Formation Dynamics through Curvature Measurements. *Journal of Thermal Spray Technology*. 2016, 25, 1666-1683.

[11] FARROKHPANAH, A., COYLE, T., MOSTAGHIMI, J., Numerical study of suspension plasma spraying. *Journal of Thermal Spray Technology*. 2017, 26, 12-36.

[12] ZHENG, B., LUO, Y., LIAO, H., ZHANG, CH. Investigation of the crystallinity of suspension plasma sprayed hydroxyapatite coatings. *Journal of the European Ceramic Society*. 2017, 37, 5017-5021.

[13] DYSHLOVENKO, S., PATEYRON, B., PAWLOWSKI, L., MURANO, D. Numerical simulation of hydroxyapatite powder behaviour in plasma jet. *Surface and Coatings Technology*. 2004, 179, 110-117.

[14] PILLAI, R.S., FRASNELLI, M., SGLAVO, V.M. HA/ β -TCP plasma sprayed coatings on Ti substrate for biomedical applications. *Ceramics International*. 2018, 44, 1328-1333.

[15] CARRODEGUAS, R.G., AZA, S.D. A-Tricalcium phosphate: Synthesis, properties and biomedical applications. *Acta Biomaterialia*. 2011, 7, 3536-3546.

[16] SADAT-SHOJAI, M., KHORASANI, M.T., DINPANAH-KHOSHDARGI, E., JAMSHIDI, A. Synthesis methods for nanosized hydroxyapatite with diverse structures. *Acta Biomaterialia*. 2013, 9, 7591-7621.

[17] JAWORSKI, R., PIERLOT, CH., PAWLOWSKI, L., BIGAN, M., MARTEL, M. Design of the synthesis of fine HA powder for suspension plasma spraying. *Surface and Coatings Technology*. 2009, 203, 2092-2097.

[18] JINLONG, N., ZHENXI, Z., DAZONG, J. Investigation of Phase Evolution During the Thermochemical Synthesis of Tricalcium Phosphate. *Journal of Materials Synthesis and Processing*. 2001, 9, 235-240.

[19] CARRODEGUAS, R.G, DE AZA, A.H., TURRILLAS, X., PENA P., DE AZA S. New approach to the beta-alpha polymorphic transformation in magnesium-substituted tricalcium phosphate and its practical implications. *Journal of the American Ceramic Society*. 2008, 91, 1281–1286.

[20] ENDERLE, R, GÖTZ-NEUNHOEFFER F., GÖBBELS, M., MÜLLER, F.A., GREIL P. Influence of magnesium doping on the phase transformation temperature of b-TCP ceramics examined by Rietveld refinement. *Biomaterials*. 2005, 26, 3379–3384.

[21] KÜHN, G., WEST, A.R. Solid state chemistry and its applications. Chichester: John Wiley, New York, 1984, ISBN 0–471–90377–9.

[22] BOHNER, M., LEMAITRE, J., LEGRAND, A.P., de la CAILLERIE, J.B.D., BELGRAND, P. Synthesis, Xray diffraction and solid-state P-31 magic angle spinning NMR study of alpha-tricalcium orthophosphate. *Journal of Materials Science: Materials in Medicine*. 1996, 7, 457–63.

[23] DAVIS, J.R. Introduction to Thermal Spray Processing. Handbook of Thermal Spray Technology. ASM International, 2004. 3-13. ISBN 0-87170-795-0.

[24] MOREAU, CH., LAMONTAGNE, M., CIELO, P. Influence of the coating thickness on the cooling rates of plasma-sprayed particles impinging on a substrate. *Surface and Coating Technologies*, 53, 1992, 107-114.

[25] VAHABZADEH, S., ROY, M., BANDYOPADHYAY, A., BOSE, S. Phase stability and biological property evaluation of plasma sprayed hydroxyapatite coatings for orthopedic and dental applications. *Acta Biomaterialia*. 2015, 17, 47-55.

[26] SUN, L., BERNDT, CH.C., KHOR, K.A., CHEANG, H.N., GROSS, K.A. Surface characteristics and dissolution behavior of plasma-sprayed hydroxyapatite coating. *Journal of Biomedical Materials Research*. 2002, 62, 228-236.

[27] REIGSTAD, O., JOHANSSON, C., STENPORT, V., WENNERBERG, A., REIGSTAD, A., RØKKUM, M. Different patterns of bone fixation with hydroxyapatite and resorbable CaP coatings in the rabbit tibia at 6, 12, and 52 weeks. *Journal of Biomedical Materials Research Part B: Applied Biomaterials*. 2011, 99, 14-20.

[28] BOLELLI, G., BELLUCCI, D., CANNILLO, V. Suspension thermal spraying of hydroxyapatite: Microstructure and in vitro behaviour. *Materials Science and Engineering: C*. 2014, 34, 287-303.

[29] ROUAHI, M., CHAMPION, E., HARDOUIN, P., ANSELME, K. Quantitative kinetic analysis of gene expression during human osteoblastic adhesion on orthopaedic materials. *Biomaterials*. 2006, 27, 2829-2844.

[30] HACKING, S.A., BOYRAZ, P., POWERS, B.M., SEN-GUPTA, E., KUCHARSKI, W., BROWN, C.A., COOK, E.P. Surface roughness enhances the osseointegration of titanium headposts in non-human primates. *Journal of Neuroscience Methods*. 2012, 211, 237-244.

[31] HEIMANN, R.B. Thermal spraying of biomaterials. *Surface and Coatings Technology*. 2006, 201, 2012-2019.

[32] BORSARI, V., FINI, M., GIAVARESI, G. Osteointegration of titanium and hydroxyapatite rough surfaces in healthy and compromised cortical and trabecular bone: in vivo comparative study on young, aged, and estrogen-deficient sheep. *Journal of Orthopaedic Research*. 2007, 25, 1250-1260.